Recoil-ion momentum distribution for nonsequential double ionization of Xe in intense midinfrared laser fields

YanLan Wang,[1,2] SongPo Xu,[1,2] Wei Quan,[1] Cheng Gong,[1] XuanYang Lai,[1] ShiLin Hu,[3] MingQing Liu,[3] Jing Chen,[3,*] and XiaoJun Liu[1,†]

[1]*State Key Laboratory of Magnetic Resonance and Atomic and Molecular Physics, Wuhan Institute of Physics and Mathematics, Chinese Academy of Sciences, Wuhan 430071, China*

[2]*University of Chinese Academy of Sciences, Beijing 100049, China*

[3]*HEDPS, Center for Applied Physics and Technology, Peking University, Beijing 100084, China and Institute of Applied Physics and Computational Mathematics, P. O. Box 8009, Beijing 100088, China*

(Received 8 September 2016; published 14 November 2016)

We experimentally investigate the recoil-ion momentum distribution along the laser polarization direction for nonsequential double ionization of Xe by 50 fs, 2400 nm laser pulses at intensities of (22−68) TW/cm^2. The observed doubly charged ion momentum distribution exhibits a distinct transition from a flat-top structure near zero longitudinal momentum at 22 TW/cm^2 to the one with two maxima at nonzero longitudinal momentum at 37 TW/cm^2, 52 TW/cm^2, and 68 TW/cm^2, which is remarkably different from the case of 800 nm. Simulation based on a semiclassical model is used to obtain the ratios of contributions from the recollision-impact ionization (RII) and the recollision-induced excitation with subsequent field ionization (RESI) in nonsequential double ionization. Our calculation reveals that the increasing contribution of the RII channel is responsible for the more prominent double-hump structure at longer wavelength or higher laser intensity. Moreover, a simple fitting based on the calculated ratios allows one to reproduce the experimental ion momentum distributions well and obtain contributions from these two channels.

DOI: 10.1103/PhysRevA.94.053412

I. INTRODUCTION

Since nonsequential double ionization (NSDI) [1] of atoms provides an ideal prototype to investigate the electron-electron correlation effect in laser-driven atomic phenomena, it has attracted increasing attention in the strong-field physics community for more than three decades (for recent reviews, see, e.g., Refs. [2–4]). Earlier experiments on ellipticity dependence of ions yields exhibit a rapid decreasing doubly charged ion yields with respect to the ellipticity [5,6], providing the first experimental evidence that the electron rescattering model is the physical mechanism of NSDI [7,8]. The rescattering mechanism can be described as three steps: firstly, the outmost electron tunnels through the distorted Coulomb potential barrier formed by the atomic potential and the intense laser field. Secondly, the freed electron propagates in the strong laser field. Finally, after the field changes sign, the electron may be driven back to recollide with the parent ion and both electrons become ionized. According to the rescattering model, there are two channels contributing to the NSDI: one is recollision-impact ionization (RII). In this channel, the bound electron may directly gain enough energy by recollision to be ionized, which is most likely to occur at the crossing of the external laser field. Thus the electrons will acquire substantial momentum along the laser polarization direction. As a consequence, the momentum distribution of the doubly charged ions would show a pronounced double-hump structure. The other is the recollision-induced excitation with subsequent field ionization (RESI). In contrast to the RII, the RESI corresponds to that the bound electron is excited firstly by the recollision and then is ionized via tunneling at the maximum of the subsequent cycle of the laser field [9]. As a result, one of the electrons will achieve very small momenta and the momentum distribution of the doubly charged ions may exhibit a single maximum at zero momentum.

With the advent of the experimental technique denoted cold-target recoil-ion momentum spectroscopy (COLTRIMS) [10], the double-hump structure in the doubly charged ion momentum distribution along the laser polarization direction has been firstly observed for He and Ne [11,12], providing solid evidence for the RII channel introduced by the rescattering model. Later, investigations for different noble gas atoms suggest that the momentum distribution is target specific [9,13–15]. A detailed comparison of the ion momentum distributions along the laser polarization direction for different noble gas atoms near 800 nm wavelength shows that the double-hump structure is most pronounced for Ne, while much less apparent or even absent for He and Ar. This phenomenon has been explained to be due to the different strength of contributions from the RII and the RESI channels, i.e., RESI plays a decisive role for He and Ar, whereas for Ne, RII clearly dominates. Recently, owing to the great advances in ultrafast laser technology, strong field physics experiments are experiencing a shift towards the use of longer wavelengths, e.g., mid-infrared wavelengths [16–20], which provides an opportunity to explore the NSDI mechanisms in a different laser-wavelength regime. Preliminary results have shown a strong dependence of the recoil ion momentum on the laser wavelength. For example, the experimental studies on Ar at longer wavelengths, e.g., around 1300 and 2000 nm, have found a pronounced double-hump structure in longitudinal ion momentum distribution [21,22], which can hardly be observed in the earlier results at 800 nm.

*chen_jing@iapcm.ac.cn
†xjliu@wipm.ac.cn

 ©2016 American Physical Society

It is noteworthy that previous studies of the recoil ion momentum distribution and the related discussions on the underlying physics behind NSDI have concentrated on noble gas atoms of He, Ne, and Ar. This is most probably due to the fact that these species have rather high ionization potentials, and thus the nonsequential regime of double ionization (DI) can be easily covered experimentally even at near-infrared wavelength, i.e., 800 nm with the commonly employed Ti:sapphire laser. In contrast, for the high-Z atomic species, e.g., Xe, the relatively low ionization potential sets a stringent limit on the experimental conditions (e.g., the maximal laser intensity due to the ionization saturation) for which the nonsequential regime can be accessed, in particular with near-infrared laser fields. This frustrates a systematic inspection of the ion momentum distribution and a comprehensive understanding of the NSDI mechanism of Xe. For example, recent experiment on the double ionization of Xe at a wavelength of 790 nm in a rather broad intensity range (i.e., $0.4–3\times10^{14}\,\mathrm{W/cm^2}$) always shows a clear Gaussian-like ion momentum distribution with the maximum at zero momentum [23], independent of the laser intensities employed. This may suggest a different ionization mechanism of Xe from the well-studied low-Z atomic rare gases. Actually, for higher laser intensities, double ionization of Xe enters into a sequential region, and one can expect a single-peak structure in the ion momentum distribution. For lower laser intensities where NSDI should dominate, the appearance of the single-peak structure has been explained by multiple rescattering and shielding effect of the high-Z atoms. In contrast, very recent experiments by Wolter *et al.* [20], performed at a wavelength of 3100 nm and an intensity of $0.4\times10^{14}\,\mathrm{W/cm^2}$, have found a pronounced double-hump structure in the longitudinal momentum distribution of the Xe^{2+}. This feature is suggested as an indication that both NSDI pathways, i.e., RII and RESI, are also present for Xe, similar to the well-studied low-Z targets. Nevertheless, how the ion momentum distribution for high-Z atom of Xe evolves with the laser parameters (e.g., laser intensity and wavelength) and, under which conditions the double-hump structure can be formed, have been hardly addressed. Therefore, a systematic inspection of the evolution of the recoil ion momentum distribution of Xe, in particular with mid-infrared laser fields, which will provide a deep insight into the physical mechanism behind NSDI of Xe, is still in demand.

In this paper, we present a systematic investigation on the recoil-ion momentum distribution along the laser polarization direction for NSDI of Xe by intense laser field at 2400 nm. At this wavelength, the ion momentum distribution exhibits a distinct transition from a flat-top structure near zero longitudinal momentum at $22\,\mathrm{TW/cm^2}$ to the one with two maxima at nonzero longitudinal momentum at $37\,\mathrm{TW/cm^2}$, $52\,\mathrm{TW/cm^2}$, and $68\,\mathrm{TW/cm^2}$. Our experimental observation indicates that the RII may play a more and more important role in the NSDI of Xe for longer wavelength and higher laser intensity. A simulation based on a semiclassical model allows us to disentangle the contributions from the RII and RESI channels in NSDI. Moreover, a quantitative analysis for the different shapes in ion momentum distributions of Xe at different laser intensities have been made, facilitating a comprehensive understanding of NSDI process of Xe at mid-infrared wavelength.

This paper is organized as follows. In Sec. II we introduce the experimental setup. In Sec. III we present experimental results, introduce a semiclassical model to disentangle the contributions from the RII and RESI channels and discuss the mechanism of NSDI in different laser wavelengths and laser intensities. Finally, in Sec. IV our conclusions are given. Atomic units (a.u.) are used throughout unless otherwise indicated.

II. EXPERIMENTAL SETUP

In our experiment, linearly polarized 2400 nm mid-infrared femtosecond laser pulses are generated by an optical parametric amplifier (TOPAS-C, Light Conversion, Inc.) pumped by a commercial Ti:sapphire laser system (Legend, Coherent, Inc.). The pulse duration is about 55 fs, and the pulse energy of up to 400 μJ from the optical parametric amplifier is achieved at 1 kHz repetition rate. The pulse energy can be varied, before being focused into the interaction chamber, by means of an achromatic half-wave plate followed by a polarizer. The laser intensity is calibrated with a procedure utilizing photoelectron (photoion) momentum distribution in circularly polarized laser fields [24,25]. The momentum distributions of the ions are measured with a newly built COLTRIMS [26,27]. The laser beam is focused by an on-axis spherical mirror ($f = 75$ mm) onto the cold collimated supersonic gas jet in the ultra-high vacuum chamber. The photoions produced in the laser-supersonic beam interaction area are accelerated by a homogeneous weak electric field (about 15.8 V/cm) towards a Microchannel Plates (MCP) detector equipped with a delay line anode (DLD80, RoentDek Handels GmbH). The detector can resolve the impact positions and the time-of-flights of the photoions, from which all the momentum vectors of the ions can be retrieved.

III. RESULTS AND DISCUSSION

Figure 1 shows the experimentally measured ion momentum distributions of Xe^{2+} along the laser polarization direction at 2400 nm for various laser intensities, i.e., $22\,\mathrm{TW/cm^2}$, $37\,\mathrm{TW/cm^2}$,$52\,\mathrm{TW/cm^2}$, and $68\,\mathrm{TW/cm^2}$. Note that there are nine stable isotopes for Xe. In this paper, we select the double ionization events of ^{129}Xe isotope to analyze the ion momentum distribution of Xe^{2+}. The general feature of the ion momentum distribution of Xe^{2+} is that doubly charged ions are symmetrically distributed with respect to zero momentum. However, a closer inspection reveals some significant differences in the ion momentum distributions from Figs. 1(a) to 1(d), with the increasing laser intensity. In the case of $22\,\mathrm{TW/cm^2}$ [Fig. 1(a)], the distribution shows a flat-top structure near zero longitudinal momentum, while at higher laser intensity, e.g., $37\,\mathrm{TW/cm^2}$ [Fig. 1(b)], the ion momentum distribution of Xe^{2+} exhibits a clear two-maxima structure at nonzero longitudinal momentum which becomes more significant as the laser intensity increases to $52\,\mathrm{TW/cm^2}$ and $68\,\mathrm{TW/cm^2}$ [see Figs. 1(c) and 1(d)]. This prominent double-hump structure at $37\,\mathrm{TW/cm^2}$, $52\,\mathrm{TW/cm^2}$, and $68\,\mathrm{TW/cm^2}$ is in striking contrast to a previous experimental result at 800 nm, where the double-hump structure is absent over a wide range of laser intensity from 40 $\mathrm{TW/cm^2}$ to

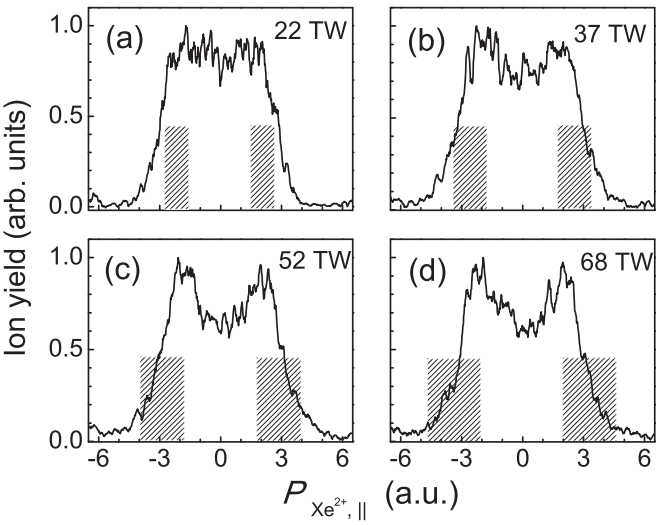

FIG. 1. Experimental ion momentum distributions of Xe^{2+} along the laser polarization direction at 2400 nm with peak intensities from 22 TW/cm^2 to 68 TW/cm^2. Note that intensities in TW/cm^2 are given here. The shaded areas indicate the kinematical allowed region of the doubly charged ion momentum for RII channel derived from the classical rescattering model [28].

300 TW/cm^2 [23]. In the earlier 800 nm experiment, the ion momentum distributions show a clear Gaussian-like structure with one single maximum at zero momentum and the shape of the spectra exhibits a weak intensity dependence. This distinction could indicate possible different NSDI mechanisms at the two wavelengths.

To qualitatively explain the above observations of ion momentum distributions at 2400 nm, we present a kinematical allowed region of the doubly charged ion momentum for the RII channel derived from the classical rescattering model, in which only the most probable kinetic energy of the rescattered electron of $3.17U_p$ and the maximal drift momentum of $4\sqrt{U_p}$ are considered [28],

$$4\sqrt{U_p} - \sqrt{2(3.17U_p - I_p^+)} \leqslant P_{Xe^{2+},||} \leqslant 4\sqrt{U_p}, \quad (1)$$

where $U_p = F_0^2/4\omega^2$ is the ponderomotive potential and I_p^+ is the ionization potential of Xe^+. Here ω and F_0 are the laser frequency and field strength. This kinematical favored region for the doubly charged ion momentum from the RII process is depicted in Fig. 1 with shaded areas in ion momentum distribution of each laser intensity. It can be clearly seen that the scaling of ion yields in shaded areas is increasing, which indicates that the RII channel becomes more and more important compared to the RESI channel with increasing intensity. It is well known that for the RII, the ions are most likely produced with nonzero momenta, while for the RESI, the ions are produced with very small momenta close to zero. The increasing relative contribution of RII makes the overall shape of momentum distribution display a clearer double-hump structure at higher laser intensity.

To shed more light on the physical mechanism behind NSDI of Xe at 2400 nm, it is desirable to quantitatively evaluate the contributions of these two channels, respectively. Thus in the remaining part of this paper, we resort to a semiclassical model suggested in Refs. [14,21], which has been successfully used to analyze the double ionization mechanism of noble gas atoms, e.g., Ne and Ar.

This semiclassical model is based on the electron recollision scenario [29]. In this scenario, the outmost electron is assumed to be released into the continuum by tunneling at time t_0. Then the freed electron propagates in the strong laser field $F(t) = F_0 \sin(\omega t)$ and may be driven back to the parent ion at time t_1 with a classical recollision energy $E_{\rm Rec} = 0.5F_0^2\omega^{-2}[\cos(\omega t_0) - \cos(\omega t_1)]^2$. Upon recollision the bound electron may directly gain enough energy to be ionized (RII) or excited followed by ionization at next maximum of laser field (RESI). The relative contributions of these two channels can be calculated by the ratio, R, of the effective (phase averaged) yields for ionization, $Y_{\rm Ion}$, and excitation, $Y_{\rm Exc}$. Here we use the following formulas [21]:

$$R = \frac{Y_{\rm Ion}}{Y_{\rm Exc}}, \quad (2)$$

$$Y_{\rm Ion(Exc)} = \int_{\pi/2}^{\pi} W_{\rm ADK}(\omega t_0) P_{\rm Ion(Exc)}\, d(\omega t_0), \quad (3)$$

where $W_{\rm ADK}(\omega t_0)$ is the ADK tunneling rate [30,31]. $P_{\rm Ion(Exc)}$ denotes the probability of the RII (RESI). The probability of ionization and excitation can be written as

$$P_{\rm Ion(Exc)} = \sigma_{\rm Ion(Exc)}(E_{\rm Rec}) \frac{1}{\pi[R(t_1 - t_0)]^2}. \quad (4)$$

Here $\sigma_{\rm Ion(Exc)}$ is the electron impact ionization (excitation) cross section. The term of $\pi[R(t_1 - t_0)]^2$ denotes transverse diffusion of the tunnel-ionized electron wave packet, which is a rough estimation for an effective cross section. It can be determined by using the mean value of transverse momentum, $\bar{p}_\perp$ and the travel time of the tunnel-ionized electron before it recollides with the parent ion $(t_1 - t_0)$:

$$R(t_1 - t_0) = \frac{1}{m_e} \bar{p}_\perp (t_1 - t_0). \quad (5)$$

Here m_e is the mass of the electron. $\bar{p}_\perp$ can be obtained by the width of a Gaussian distribution [30,31]:

$$\bar{p}_\perp = \tfrac{1}{2}\sqrt{F_0/\sqrt{8I_p}}, \quad (6)$$

where I_p is ionization potential of atom. Thus, the integral for $Y_{\rm Ion(Exc)}$ becomes

$$Y_{\rm Ion(Exc)} = \int_{\pi/2}^{\pi} W_{\rm ADK}(\omega t_0)\sigma_{\rm Ion(Exc)}(E_{\rm Rec}) \times \frac{8m_e^2\omega^2\sqrt{2I_p}}{\pi(\omega t_1 - \omega t_0)^2 F_0}\, d(\omega t_0). \quad (7)$$

Apparently, the contributions of RII and RESI are largely determined by the cross section of electron impact ionization and excitation, which are calculated by using a simplified (field-free) formula [14,32],

$$\sigma_{\rm Ion(Exc)}(E_{\rm Rec}) = \sum_{lk} C_l \left(\frac{Ryd}{I_p^{+(k)}}\right)^{2-\delta_l} \xi_l b_k \times \frac{\ln\left[1 + \left(E_{\rm Rec} - \tilde{I}_p^{+(k)}\right)/I_p^{+(k)}\right]}{E_{\rm Rec}/I_p^{+(k)}}, \quad (8)$$

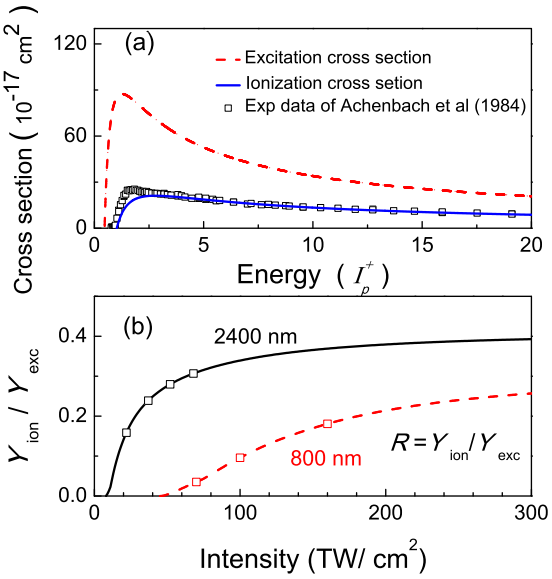

FIG. 2. (a) Calculated impact excitation cross section (dashed red line) and calculated electron impact ionization cross section (solid blue line). The experimental ionization cross section of Achenbach *et al.* [34] is shown with black squares for comparison. (b) Calculated ratios of the NSDI yields of RII and the RESI at 800 nm (dashed red line) and 2400 nm (solid black line) as a function of the laser intensity. The squares in (b) represent ratios at laser intensities used in this paper and a previous work [23].

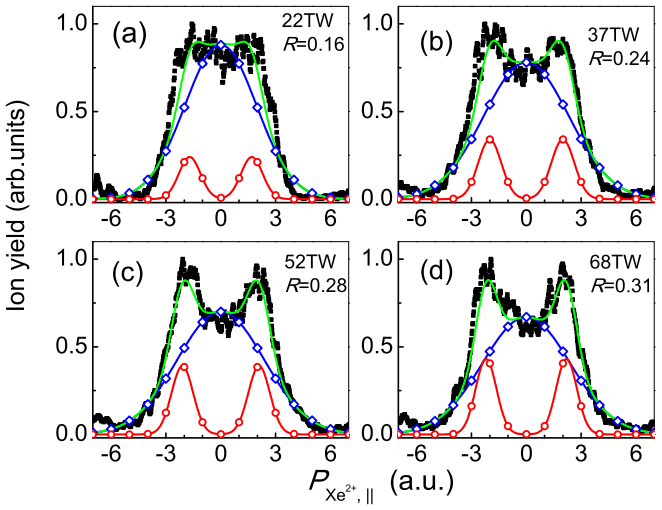

FIG. 3. Separated contributions of the longitudinal momentum distributions of Xe^{2+} from different recollision-induced channels of double ionization at various intensities by applying a fitting procedure. Black squares: experimental data. Red curves with circles: RII contributions. Blue curves with diamonds: RESI contributions. Green solid curves: total fits of the experimental data. Note that intensities in TW/cm^2 and calculated ratios R are given.

where the coefficients C_l and δ_l can be obtained in Ref. [32]. Ryd = 13.6 eV is the Rydberg constant. ξ_l is the number of equivalent electrons in the initial l subshell. b_k is the probability for ionization into a specific final state of term k, i.e., branching ratio. $\tilde{I}_p^+ = I_p^+ - 2\sqrt{2F(t_1)}$ is the suppressed ionization potential of the ion [33], which is introduced to consider the effect of barrier suppression resulting from a finite field at the recollision time t_1. In this work, for ionization cross section, the $5p$ and $5s$ subshells are included in our calculation. For the impact excitation case, we use the $5s5p^6$ excitation, which has the largest impact excitation cross section in Xe to account for Xe^{2+} yield and $(Xe^+)^*$ is assumed to ionize with unity probability. In Fig. 2(a) we show the calculated cross sections of excitation and electron impact ionization as a function of incident electron energy in units of ionization potential of Xe^+. Note that the experimental ionization cross section of Achenbach *et al.* [34] is also shown with black squares for comparison.

Furthermore, the calculated relative ratios of the double ionization yields of the RII and RESI as a function of the laser intensity are shown in Fig. 2(b) for 800 nm (dashed red line) and 2400 nm (solid black line), in which the ratios at laser intensity used by this paper and previous work in Ref. [23] are indicated with squares. The results clearly show an increasing ratio with the increasing laser intensity for both two wavelengths, which can be explained with the increasing rescattering energy determined by the ponderomotive potential U_p at higher laser intensity. As a result, the increasing contribution of RII leads to a more and more prominent double-hump structure with increasing intensity at 2400 nm. The differences between the ion momentum distributions at 800 nm and 2400 nm can also be explained with the calculated ratios. It is easy to understand that the ratio is always larger for 2400 nm than 800 nm at the same laser intensity considering a larger U_p at 2400 nm. Compared to the 2400 nm case, for 800 nm, it is harder to reach a high contribution for RII. For example, at the high laser intensity of 160 TW/cm^2 where the NSDI process still dominates in the yields of Xe^{2+}, R is only 0.18, which is still less than the case for 2400 nm at a much lower laser intensity of 37 TW/cm^2 where R already reaches 0.24. Increasing the laser intensity may increase the ratio even further. As shown in our calculations, $R = 0.24$ for 250 TW/cm^2 [see Fig. 2(b)] at 800 nm. However, note that, for this high intensity, another DI mechanism, i.e., the sequential ionization, should play a major role in the production of a doubly charged ion of Xe [35–37] and the two electrons will be released sequentially. It is worth mentioning that, for the lower laser intensities at 800 nm used in the previous work [23], $R = 0.1$ for 100 TW/cm^2 and $R < 0.1$ for 70 and 40 TW/cm^2, suggesting that RESI channel always plays a decisive role in the NSDI process of Xe. This may explain the persistence of the single-peak structure in the ion momentum distribution observed for Xe^{2+} at 800 nm and the relatively weak intensity dependence of the structure.

Based on the calculated ratios R, we can separate these two channels in the experimental ion momentum distributions by applying a fitting procedure [21], as shown in Fig. 3. In the fitting procedure, we use a Gaussian peaked at zero momentum (blue curve with diamonds) and a two Gaussian centered at some nonzero momenta curve (red curve with circles), respectively. By using appropriate ratios for each laser intensities, i.e., $R = 0.16$ for 22 TW/cm^2, $R = 0.24$ for 37 TW/cm^2, $R = 0.28$ for 52 TW/cm^2, and $R = 0.31$ for 68 TW/cm^2, the experimental ion momentum distributions data are well reproduced by the simple fitting. Therefore, the

different shapes of the ion momentum spectra for NSDI of Xe at different laser intensities can be understood by considering the relative contributions from the two distinct electron recollison pathways, i.e., RII and RESI, without introducing other effects, e.g., shielding of other electrons in the atom.

IV. CONCLUSION

In conclusion, the recoil-ion momentum distributions along the laser polarization direction for NSDI of Xe by intense laser field at 2400 nm is studied. It is found that the doubly charged ion momentum distribution exhibits a distinct transition from a flat-top structure near zero longitudinal momentum at 22 TW/cm^2 to the one with two maxima at nonzero longitudinal momentum at 37 TW/cm^2, 52 TW/cm^2, and 68 TW/cm^2. This observation is remarkably different from the 800 nm case. Quantitative simulations based on a semiclassical model can be used to obtain the ratios of the contributions from the RII and the RESI in NSDI. Simulation reveals that the increasing contribution of RII is responsible for the more prominent double-hump structure at longer wavelength or higher laser intensity. Moreover, a simple fitting based on the calculated ratios allows one to reproduce the experimental data of the ion momentum distribution and obtain separated contributions from these two channels, indicating that the underlying mechanism of the NSDI of Xe is similar to that of other lighter noble gas atoms, e.g., He, Ne, and Ar.

ACKNOWLEDGMENTS

This work is supported by the National Basic Research Program of China (Grant No. 2013CB922201), the NNSF of China (Grants No. 11334009, No. 11204356, No. 11374329, No. 11474321, No. 11274050, and No. 11425414) and the Youth Innovation Promotion Association of CAS (2011242).

[1] D. N. Fittinghoff, P. R. Bolton, B. Chang, and K. C. Kulander, Phys. Rev. Lett. **69**, 2642 (1992).
[2] A. Becker, R. Dörner, and R. Moshammer, J. Phys. B **38**, S753 (2005).
[3] C. Faria and X. Liu, J. Mod. Opt. **58**, 1076 (2011).
[4] W. Becker, X. Liu, P. Ho, and J. H. Eberly, Rev. Mod. Phys. **84**, 1011 (2012).
[5] D. N. Fittinghoff, P. R. Bolton, B. Chang, and K. C. Kulander, Phys. Rev. A **49**, 2174 (1994).
[6] P. Dietrich, N. H. Burnett, M. Ivanov, and P. B. Corkum, Phys. Rev. A **50**, R3585 (1994).
[7] P. B. Corkum, Phys. Rev. Lett. **71**, 1994 (1993).
[8] K. C. Kulander, K. J. Schafer, and J. L. Krause, in *Super-Intense Laser-Atom Physics*, edited by B. Piraux, A. L'Huillier, and K. Rzążewski (Plenum, New York, 1993), p. 95.
[9] B. Feuerstein, R. Moshammer, D. Fischer, A. Dorn, C. D. Schroter, J. Deipenwisch, J. R. CrespoLopez-Urrutia, C. Hohr, P. Neumayer, J. Ullrich, H. Rottke, C. Trump, M. Wittmann, G. Korn, and W. Sandner, Phys. Rev. Lett. **87**, 043003 (2001).
[10] J. Ullrich, R. Moshammer, A. Dorn, R. Dörner, L. Ph. Schmidt, and H. Schmidt-Böcking, Rep. Prog. Phys. **66**, 1463 (2003).
[11] T. Weber, M. Weckenbrock, A. Staudte, L. Spielberger, O. Jagutzki, V. Mergel, F. Afaneh, G. Urbasch, M. Vollmer, H. Giessen, and R. Dorner, Phys. Rev. Lett. **84**, 443 (2000).
[12] R. Moshammer, B. Feuerstein, W. Schmitt, A. Dorn, C. D. Schroter, J. Ullrich, H. Rottke, C. Trump, M. Wittmann, G. Korn, K. Hoffmann, and W. Sandner, Phys. Rev. Lett. **84**, 447 (2000).
[13] A. Rudenko, K. Zrost, B. Feuerstein, V. L. B. de Jesus, C. D. Schröter, R. Moshammer, and J. Ullrich, Phys. Rev. Lett. **93**, 253001 (2004).
[14] V. L. B. de Jesus, B. Feuerstein, K. Zrost, D. Fischer, A. Rudenko, F. Afaneh, C. D. Schröter, R. Moshammer, and J. Ullrich, J. Phys. B **37**, L161 (2004).
[15] Y. Q. Liu, S. Tschuch, A. Rudenko, M. Dürr, M. Siegel, U. Morgner, R. Moshammer, and J. Ullrich, Phys. Rev. Lett. **101**, 053001 (2008).
[16] P. Colosimo *et al.*, Nat. Phys. **4**, 386 (2008).
[17] C. I. Blaga, F. Catoire, P. Colosimo, G. G. Paulus, H. G. Muller, P. Agostini, and L. F. Dimauro, Nat. Phys. **5**, 335 (2009).
[18] W. Quan, Z. Lin, M. Wu, H. Kang, H. Liu, X. Liu, J. Chen, J. Liu, X. T. He, S. G. Chen, H. Xiong, L. Guo, H. Xu, Y. Fu, Y. Cheng, and Z. Z. Xu, Phys. Rev. Lett. **103**, 093001 (2009).
[19] A. D. DiChiara, E. Sistrunk, C. I. Blaga, U. B. Szafruga, P. Agostini, and L. F. DiMauro, Phys. Rev. Lett. **108**, 033002 (2012).
[20] B. Wolter, M. G. Pullen, M. Baudisch, M. Sclafani, M. Hemmer, A. Senftleben, C. D. Schroter, J. Ullrich, R. Moshammer, and J. Biegert, Phys. Rev. X **5**, 021034 (2015).
[21] O. Herrwerth *et al.*, New J. Phys. **10**, 025007 (2008).
[22] A. S. Alnaser, D. Comtois, A. T. Hasan, D. M. Villeneuve, J. C. Kieffer, and I. V. Litvinyuk, J. Phys. B **41**, 031001 (2008).
[23] X. Sun, M. Li, D. Ye, G. Xin, L. Fu, X. Xie, Y. Deng, C. Wu, J. Liu, Q. Gong, and Y. Liu, Phys. Rev. Lett. **113**, 103001 (2014).
[24] A. S. Alnaser, X. M. Tong, T. Osipov, S. Voss, C. M. Maharjan, B. Shan, Z. Chang, and C. L. Cocke, Phys. Rev. A **70**, 023413 (2004).
[25] C. Smeenk *et al.*, Opt. Exp. **19**, 9336 (2011).
[26] Y. J. Chen, S. G. Yu, R. P. Sun, C. Gong, L. Q. Hua, X. Y. Lai, W. Quan, and X. J. Liu, Chin. Phys. Lett. **33**, 043301 (2016).
[27] W. Quan *et al.*, Sci. Rep. **6**, 27108 (2016).
[28] B. Feuerstein, R. Moshammer, and J. Ullrich, J. Phys. B **33**, L823 (2000).
[29] G. G. Paulus, W. Becker, W. Nicklich, and H. Walther, J. Phys. B **27**, L703 (1994).
[30] M. V. Ammosov, N. B. Delone, and V. P. Krainov, Zh. Eksp. Teor. Fiz. **91**, 2008 (1986) [Sov. Phys. JETP **64**, 1191 (1986)].
[31] N. B. Delone and V. P. Krainov, Phys. Usp. **41**, 469 (1998).
[32] V. A. Bernshtam, Yu.V. Ralchenko, and Y. Maron, J. Phys. B **33**, 5025 (2000).
[33] H. W. van der Hart and K. Burnett, Phys. Rev. A **62**, 013407 (2000).
[34] C. Achenbach, A. Müller, E. Salzborn, and R. Becker, J. Phys. B **17**, 1405 (1984).
[35] J. Rudati, J. L. Chaloupka, P. Agostini, K. C. Kulander, and L. F. DiMauro, Phys. Rev. Lett. **92**, 203001 (2004).

[36] Z. Y. Lin, X. Y. Jia, C. L. Wang, Z. L. Hu, H. P. Kang, W. Quan, X. Y. Lai, X. J. Liu, J. Chen, B. Zeng, W. Chu, J. P. Yao, Y. Cheng, and Z. Z. Xu, Phys. Rev. Lett. **108**, 223001 (2012).

[37] H. P. Kang, Z. Y. Lin, S. P. Xu, C. L. Wang, W. Quan, X. Y. Lai, X. J. Liu, X. Y. Jia, X. L. Hao, J. Chen, W. Chu, J. P. Yao, B. Zeng, Y. Cheng, and Z. Z. Xu, Phys. Rev. A **90**, 063426 (2014).